The following publication Budianto, D. P. K. Lun and Y. Chan, "Robust Single-Shot Fringe Projection Profilometry Based on Morphological Component Analysis," in IEEE Transactions on Image Processing, vol. 27, no. 11, pp. 5393-5405, Nov. 2018 is available at https://doi.org/10.1109/TIP.2018.2858547.

Robust Single-shot Fringe Projection Profilometry Based on Morphological Component Analysis

Budianto, *Member, IEEE*, Daniel P.K. Lun, *Senior Member, IEEE,* and Yuk-Hee Chan, *Member, IEEE*

***Abstract*— In a fringe projection profilometry (FPP) process, the captured fringe images can be modeled as the superimposition of the projected fringe patterns on the texture of the objects. Extracting the fringe patterns from the captured fringe images is an essential procedure in FPP; but traditional single-shot FPP methods often fail to perform if the objects have a highly textured surface. In this paper, a new single-shot FPP algorithm which allows the object texture and fringe pattern to be estimated simultaneously is proposed. The heart of the proposed algorithm is an enhanced morphological component analysis (MCA) tailored for FPP problems. Conventional MCA methods which use a uniform threshold in an iterative optimization process are inefficient to separate fringe-like patterns from image texture. We extend the conventional MCA by taking advantage of the low-rank structure of the fringe's sparse representation to enable an adaptive thresholding process. It ends up with a robust single-shot FPP algorithm that can extract the fringe pattern even if the object has a highly textured surface. The proposed approach has a side benefit that the object texture can be simultaneously obtained in the fringe pattern estimation process, which is useful in many FPP applications. Experimental results have demonstrated the improved performance of the proposed algorithm over the conventional single-shot FPP approaches.**

***Index Terms*—Fringe projection profilometry, 3D model Reconstruction, morphological component analysis (MCA), Wavelets.**

I. Introduction

The fringe pattern profilometry (FPP) is an active-range three-dimensional (3D) scanning method that has been used in many computer vision applications, such as industrial modeling and inspection [2-5], 3D scene reconstruction [6-11], and 3D face scanning [12, 13], etc. The FPP method offers fast, high resolution and full-field measurements of objects' 3D information by performing triangulation between a camera and a projector. By projecting and processing sequences of time-multiplexed periodic patterns, the 3D model of an object can be derived from the phase deformation of the patterns caused by the object's geometry.

According to the number of fringe projections, FPP methods can be divided into two groups, namely, multi-shot FPP [8-10, 12, 15, 16] and single-shot FPP [1, 17-22]. The multi-shot FPP methods (such as the Phase Shifted Profilometry (PSP) [11]) are known to have a more stable performance than the single-shot ones. However, they require the projection of many fringe patterns to the target objects. And in order to achieve a complete correspondence between the projected patterns and captured images, the scene must be kept stationary during the image-acquisition process, which is not realistic in many applications of FPP. In contrast, the single-shot FPP methods can work for dynamic scenes since they only require one fringe pattern projection. Without multiple fringe patterns, single-shot FPP methods require an explicit filtering process to remove the object's textures from the fringe image. It introduces many problems related to the robustness in the implementation. Many solutions have been suggested to solve the problem. They include projecting an additional flat pattern to estimate the object texture [24, 25], but then the method is no longer single-shot. Another kind of solutions is to enhance the filtering process using for instance the Fourier transform [17, 22, 26, 27], wavelet transform [1, 18, 19, 21, 28], or heuristic approaches, such as interpolation [23] and linear compensation algorithms [29-31]. However, these approaches often fail when the target objects have vivid textures. In [23, 29-32], an interesting color-encoding PSP approach is adopted to allow the multi-shot FPP techniques to be carried out using a single-shot approach. Rather than projecting a number of fringe patterns in sequence, these fringe patterns are each encoded by a distinct color and combined into a single image to project to the object. Then by color filtering the resulting fringe image, different fringe patterns can be retrieved and the traditional multi-shot method can be performed. Although the approach can automatically remove the object texture similar to the traditional multi-shot FPP methods, the color filtering process can introduce all kinds of errors since the object can also have the same color as the fringes. There needs to be a more effective approach to separate the fringe pattern and object texture.

In this paper, a robust single-shot FPP method is proposed. By "single-shot", we mean that no additional illuminated image (either visible or non-visible) is employed. The proposed FPP

This work is fully supported by the Hong Kong Research Grant Council under research grant PolyU 5210/13E.

Budianto, Daniel P.K. Lun*, and Yuk-Hee Chan are with the Department of Electronic and Information Engineering, the Hong Kong Polytechnic University, Hung Hom, Kowloon, Hong Kong (e-mail: enpklun@polyu.edu.hk)

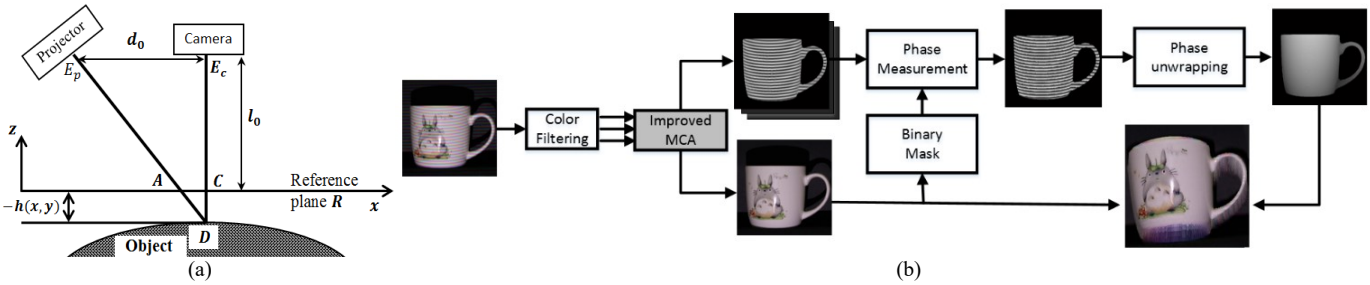

Fig. 1. (a) FPP setup in crossed optical axes geometry. (b) The single-shot FPP framework used in this work. The shaded block is the proposed MCA algorithm for separating the fringe pattern and object texture from a fringe image.

method also adopts the color-encoding PSP approach in [23, 29-32], but we improve the robustness of the method by using the morphological component analysis (MCA) [14, 33-36] to separate the fringe pattern and object texture in the captured fringe image. However, unlike the conventional MCA, we introduce a new thresholding scheme by taking advantage of the low-rank structure of the fringe's sparse representation to enable a spatially adaptive thresholding process. It ends up with a robust single-shot FPP that can better extract the fringe pattern than the conventional approaches even if the object has a highly textured surface. Besides, the proposed method does not require pre-calibration for color-coupling compensation as in the approaches in [29, 30, 37].

It should be noted that traditional single-shot FPP methods often only focus on the extraction of the fringe pattern. While the fringe pattern is essential to the reconstruction of the 3D model, the texture of the object is also an extremely useful information for many diagnostic applications of FPP. The proposed method can estimate the fringe pattern as well as object texture simultaneously, which is a side benefit in addition to the robustness it brings. A summary of the single-shot FPP framework used in this work is shown in Fig. 1b. As shown in the figure, the captured color-encoded fringe image is decoded by a color filtering process. Each decoded fringe image is decomposed into a fringe pattern and an object texture image using the proposed MCA, which will be described in detail in Section III. We then use the object texture image to generate a binary-mask that indicates the region of interest in the fringe pattern where the wrapped phase information of the object can be found. Finally, the 3D model of the object can be computed using a phase-unwrapping procedure, and the estimated object texture can also be mapped to the 3D model to facilitate different FPP applications.

The rest of this paper is organized as follows. Section II describes the principle of FPP method, color-encoding phase shifting profilometry (PSP) method, and MCA. In Section III, the details of the improved MCA for FPP method are described. Section IV reports the experimental results and finally, conclusions are drawn in Section V.

II. Background and Related Works

The proposed method involves two broad areas of study, namely, FPP and MCA. To provide an introduction of these two areas, their background and related works are outlined in the following subsections.

A. The Principle of FPP Method

In this section, the principle of FPP method is outlined. The optical setup of an FPP system with crossed optical axis geometry is shown in Fig.1a. As shown in the figure, an FPP system uses a projector to projects a fringe pattern from E_p to the target object. A camera at E_c is then used to capture the deformed fringe pattern due to the object's height profile. The camera and projector have a distance of d_0 and their lens are strictly aligned in the horizontal/vertical direction. They are placed at a distance of l_0 from a reference plane R. The fringe image captured by the camera at E_c can be modeled mathematically as a sinusoidal function as follows [17]:

$$G(x,y) = A(x,y) + B(x,y)\cos[\phi(x,y)\,], \tag{1}$$

where $G(x,y)$ represents the image pixel at spatial position (x,y); B is the local amplitude of the fringe; and A is the bias due to the reflectance of the object surface. It appears as the texture of the object in a fringe image. In (1), $\phi(x,y) = 2\pi f_0 x + \varphi(x,y)$ is the phase angle in which f_0 is the carrier frequency, and $\varphi(x,y)$ is the phase shift of the fringe in x and y directions. The object height h then can be defined as follows [17]:

$$h(x,y) \approx -\frac{l_0}{2\pi f_0 d_0}\Delta\varphi(x,y) \tag{2}$$

In (2), $\Delta\varphi(x,y) = \varphi(x,y) - \varphi_0(x,y)$, where φ_0 is the φ when there is no object. It is assumed to be known in the initial calibration process. Hence if ϕ is known, φ and also $\Delta\varphi$ can be determined. Then the object height profile h and in turn the 3D model of the object can be reconstructed. The problem is how to retrieve ϕ from the fringe image G in (1).

B. Color-Encoding PSP

Rather than projecting one fringe pattern to retrieve ϕ, the the PSP method [11], which is one of the multi-shot FPP methods, suggests to project three fringe patterns having different phase shifts to the object in sequent. The captured fringe images can then be modeled mathematically as follows:

$$G_n(x,y) = A(x,y) + B(x,y)\cos\left(\phi(x,y) - \frac{2n\pi}{3}\right), \tag{3}$$

where $n \in \{0,1,2\}$ corresponds to the three captured fringe images. It can be seen in (3) that the projected patterns have a

phase shift of $\frac{2n\pi}{3}$. The phase information ϕ in (3) can be evaluated from G_n by,

$$\hat{\phi} = arctan\left[\sqrt{3}\frac{G_0 - G_2}{2G_1 - G_0 - G_2}\right]. \quad (4)$$

It can be seen that the evaluation in (4) will not be affected by the bias term A. It thus allows the PSP method to be more robust in general than the single-shot approaches. However, the sequential projection of fringe patterns requires the object to be kept absolutely static or severe distortion will result. To solve this problem, the color-encoding PSP method suggests to encode the three phase shifted fringe patterns with different colors (such as red, green, and blue, respectively). They are combined into a single full-color image and projected onto the object. In theory, G_n can be obtained by color filtering the captured color fringe image. However, many practical problems, such as the color crosstalk and nonlinear property of the projector and camera for different colors, can introduce distortion to the colored sinusoids such that they do not follow the model in (3). Since these distortions are static, some compensation methods were developed to remove the distortion. They include using a compensation matrix [31, 37, 38] (which can be estimated with a calibration method), the generalized phase-shifting algorithm [29], or a phase error suppression method using a simple band-pass filter [30]. However, color errors can also be incurred by the reflectance of the target objects. Due to the material or color patterns on the object surface, an object can have different reflectance for different colors at different parts of the object. Such error is far more difficult to compensate since it is object dependent. To accommodate such error, (3) can be rewritten as,

$$G_n(x,y) = A_n(x,y) + B(x,y)\cos\left(\phi(x,y) - \frac{2n\pi}{3}\right), \quad (5)$$

where the bias term A_n is affected by the reflectance of the target object. Different from (3), A_n now becomes channel dependent. Thus, the phase information ϕ in (5) cannot be evaluated from G_n directly as in (4). It can only be evaluated by the second term of (5) as follows:

$$\hat{\phi} = arctan\left[\sqrt{3}\frac{G_0' - G_2'}{2G_1' - G_0' - G_2'}\right] \quad (6)$$

where $G_n(x,y) = A_n(x,y) + G_n'(x,y)$ and

$$G_n'(x,y) = B(x,y)\cos\left(\phi(x,y) - \frac{2n\pi}{3}\right). \quad (7)$$

(6) and (7) show that the phase ϕ can only be evaluated when the bias term A_n and the fringe pattern term G_n' can be well separated. Thus, we consider the task of recovering the fringe pattern from the abovementioned color errors due to the object texture as a signal separation problem. MCA is a possible tool to solve the problem since the fringe pattern and object texture have quite different morphological structures. More details of MCA are given in the next subsection.

C. MCA

In this subsection, the related work and the background of MCA are introduced. MCA is an iterative optimization process for separating the components of a signal if they have different morphological structures. It does not need to have an extremely good initial guess to guarantee the convergence of the optimization, and can give good performance with incomplete input data (due to noise or other perturbation of the system). The MCA algorithm often involves operations in both spatial and transform domains. For the ease of presentation, we will use uppercase letters to denote quantities in the spatial domain and their corresponding lowercase letters to denote their transform coefficients. Let Y be an image containing two components Y_1 and Y_2 as follows:

$$Y = Y_1 + Y_2 + N, \quad (8)$$

where N is the additive noise in the image and is assumed to be white Gaussian. Under MCA, we can recover Y_1 and Y_2 from Y by solving the following constrained optimization problem:

$$\arg\min_{y_1,y_2} \|y_1\|_1 + \|y_2\|_1 \; s.t. \; \|Y - \Phi_1^T y_1 - \Phi_2^T y_2\|_2 < \zeta, \quad (9)$$

where $\Phi_{i=1,2}$ are the dictionaries that generate the decomposition of $Y_{i=1,2}$ into $y_{i=1,2}$: $y_{i=1,2} = \Phi_{i=1,2} Y_{i=1,2}$ and ζ is the standard deviation of the noise N. Φ_i^T is the inverse of Φ_i. In (9), it is assumed that each component $y_{i=1,2}$ is associated with a sparse dictionary $\Phi_{i=1,2}$ that is mutually incoherent to each other. More specifically, for each i, y_i is only sparse in Φ_i and not, or at least not as sparse, in Φ_j, for all $j \neq i$. (9) can be solved through an iterative alternate-thresholding scheme. In each iteration of the scheme, the image is transformed with the sparse basis $\Phi_{i=1,2}$ alternately. Thus, the magnitude of the transform coefficients of component y_i should have a larger magnitude than those of component y_j for all $j \neq i$. By thresholding the transform coefficients, it is likely that more coefficients of the component y_i will be retained while those of y_j will be removed. By alternately iterating the thresholding process for different components, the errors of their estimations will be gradually reduced and they will be separated from each other when the iteration converges. Hence, one of the important parameters for determining the performance of the algorithm is the value of the thresholds.

The thresholding method of MCA has been studied in different works as it largely determines the performance of the algorithm. Various ways have been suggested to determine the threshold and how it is updated in each iteration [33, 34]. For example, in [34], the threshold is decreased linearly or exponentially toward a constant proportional to the noise variance in each iteration. To achieve a fast decomposition with the least number of iteration, [33, 34] employs an adaptive thresholding strategy which suggests the threshold can be estimated by a so-called mean of max (MOM) approach. However, the estimation is made based on the mutual incoherence assumption of the dictionaries associated to different components. Although recent developments in harmonic analysis have introduced many new multiscale transforms, it is still not possible to ensure the mutual incoherence assumption is valid in every application. If the assumption cannot be fulfilled, the optimization process of

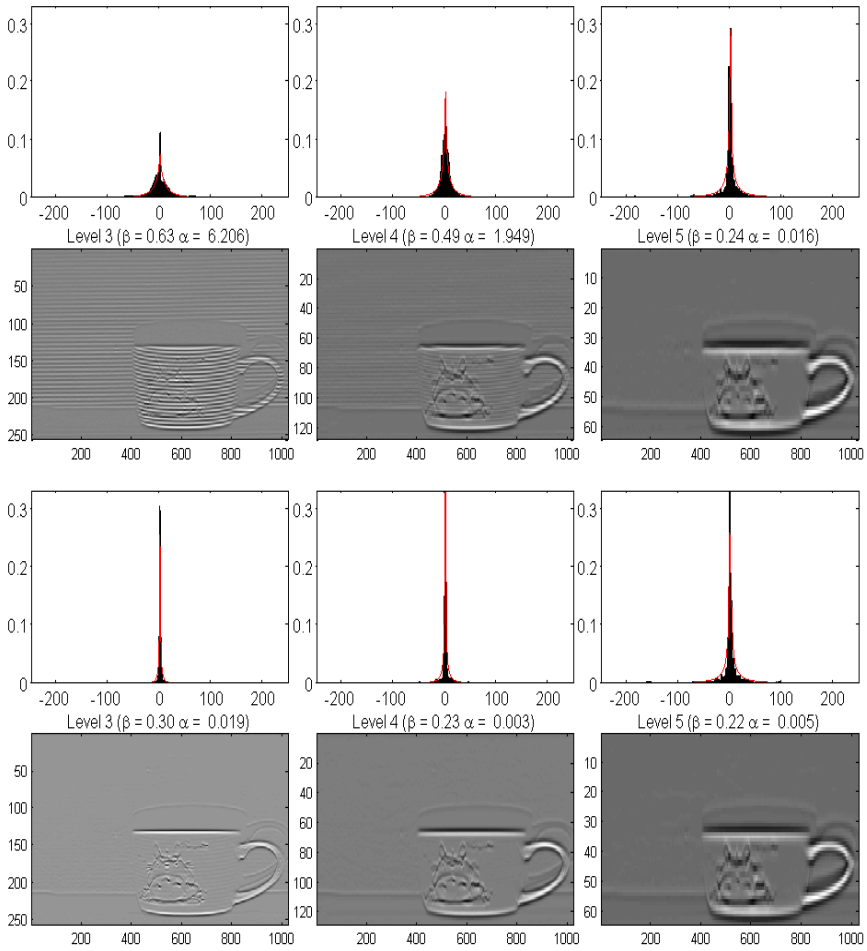

Fig. 2. TQWT coefficients (Levels 3 to 5), their histograms, and distribution fits (red curves) obtained from a fringe image (first and second rows) and a flat image of the same object with no fringe (third and fourth rows).

MCA will be lengthened or even may not converge to the desired solution. It is exactly the problem when applying MCA to FPP. First, since many FPP applications require fast, if not real-time, performance, the implementation of the dictionaries needs to have fast algorithms. Hence, there are not too many choices but only the structured transforms can meet the requirement. As we will show in Section III, the similarity in the fringe pattern and object texture introduces much difficulty in finding the required structured transforms that can fully fulfill the mutual incoherence assumption. Directly applying MCA to FPP thus often gives unsatisfactory results, particularly when the object contains strong texture. To solve the problem, we extend the conventional MCA by taking advantage of the low-rank structure of the fringe's sparse representation to enable an adaptive thresholding process. We found that although the transform coefficients of the fringe pattern and object texture cannot be directly differentiated since the transform base cannot fulfill the mutual incoherence assumption, the threshold can still be determined by their difference in regularity as reflected by their rank. As a side effect, the threshold thus obtained will be adaptive and contextual to the spatial information of the fringes. We show that this new strategy is practical and can better extract the fringe pattern than the conventional approaches even if the object has a highly textured surface.

III. IMPROVED MCA FOR FRINGE PATTERN AND OBJECT TEXTURE SEPARATION

In this section, an improved MCA algorithm for FPP is proposed. To follow the notations used in Section IIC, let Y be one of the color channels of the captured fringe image (i.e., G_n in (5)). It is composed of the object texture Y_1 (i.e., the bias term A_n in (5)) and fringe pattern Y_2 (i.e, the fringe pattern term G_n' in (5)) plus noise N. To apply MCA to estimate Y_1 and Y_2 for each color channel of the captured fringe image, we should first select an appropriate set of sparse bases $\Phi_{i=1,2}$. As mentioned above, it is required that y_i should only be sparse in Φ_i and not, or at least not as sparse, in Φ_j, for all $j \neq i$. Since many FPP applications require fast, if not real-time, performance, the implementation of $\Phi_{i=1,2}$ needs to have fast algorithms. Hence there are not too many choices but only the structured transforms can meet the requirement. Following the traditional MCA, we implement Φ_1 and Φ_2 with the tunable-Q wavelet transform (TQWT) [39] and discrete cosine transform (DCT), respectively. They both have fast algorithms. When applying to

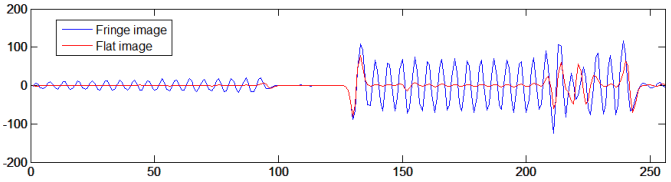

Fig. 3. The TQWT coefficients along the dashed lines in the second (blue line) and last rows (red line) of Fig. 2.

FPP, TQWT can give sparse outputs for the object texture due to the vanishing moments of its tunable Q-factor wavelet function. DCT on the other hand can give sparse outputs for the fringes due to its good frequency selectivity. Fig. 2 shows the results when applying TQWT to a fringe image. It is seen that in some scales the magnitudes of the transform coefficients of the fringe pattern and object texture are quite similar (e.g. scale 3 and 4 in the second row of Fig. 2). Both of them can be clearly seen at those scales. In fact, such result can be found when using most of the wavelet transforms. To further illustrate the above point, let us take a closer look to Fig. 3 where the TQWT coefficients along the dash lines in Fig. 2 are shown. The blue line shows the TQWT coefficients of the fringe image while the red line shows the TQWT coefficients of the object texture. It can be seen that most parts of the blue line are oscillating. They correspond to the TQWT coefficients of the fringe pattern. They have a rather large magnitude comparable to the coefficients of the object texture (red line). Now assume that we would like to set a threshold to kill the fringe coefficients in the blue line while keeping those for the object texture. A uniform threshold used in the traditional MCA algorithms obviously will be difficult to achieve task since the TQWT coefficients of the fringe pattern and object texture can have similar magnitude. The above illustrates why the traditional MCA is inefficient for FPP problems. While it is not easy to find other bases that can fulfill all the requirements as mentioned above, we suggest to change the thresholding scheme. Rather than using a uniform threshold, we propose that the threshold should be selected adaptively according to the context of each scale and spatial region. As shown in the second row of Fig. 2, not all scales of a fringe image contain both the object texture and fringe pattern components. Different thresholding schemes should then be used for different scales. And for the scales having both components (such as the case shown in Fig. 3), the thresholds at the positions where object texture's TQWT coefficients are found should be small while those at the other positions should be large. As will be discussed below, such adaptive threshold can be obtained by exploiting the low-rank property of the fringe pattern in the TQWT domain.

Let us start our discussion of the proposed MCA algorithm by looking at the optimization problem resulting from the following modification of (9).

$$\underset{y_1,y_2}{arg\ min}\ \|y_1\|_1 + \|y_2\|_1 + \ \|Y - \Phi_1^T y_1 - \Phi_2^T y_2\|_2. \tag{10}$$

The problem in (10) is commonly solved using the iterative alternate-thresholding method by updating y_1 and y_2 alternately in each iteration. More specifically, we can first focus on y_1 by fixing y_2. (10) can then be written as

$$\hat{y}_1 = \underset{y_1}{arg\ min}\|y_1\|_1 + \ \|R_1 - \Phi_1^T y_1\|_2. \tag{11}$$

In (11), $R_1 = Y - \Phi_2^T \hat{y}_2 = Y_1 + \tilde{Y}_2 + Y_n$, where $\tilde{Y}_2$ is the estimation error of Y_2 in the previous iteration. The solution of (11) can then be used to obtain $R_2 = Y - \Phi_1^T \hat{y}_1$, and then applied to the optimization of finding y_2 as follows:

$$\hat{y}_2 = \underset{y_2}{arg\ min}\|y_2\|_1 + \ \|R_2 - \Phi_2^T y_2\|_2, \tag{12}$$

It then iterates between (11) and (12) until converged. Given $r_{i=1,2} = \Phi_{i=1,2} R_{i=1,2}$, it is known that (11) and (12) can be analytically solved by using a hard thresholding operation H_{λ_i} with a threshold λ_i [14], where

$$H_{\lambda_{i=1,2}}(r_{i=1,2}) = \{r_{i=1,2}\ if\ |r_{i=1,2}| > \lambda_{i=1,2}\ and\ 0\ otherwise\}. \tag{13}$$

The performance of the algorithm is largely determined by the thresholds λ_i, which should be set proportional to the magnitude of the deviation of r_i from y_i. Traditional MCA assumes such deviation is scattered in the transform domain and has a small magnitude comparing with y_i. Hence a uniform threshold is used. However, we have shown above that such assumption is not valid for r_1, since the TQWT coefficients of the object texture and the fringe pattern can have similar magnitude for some scales. Rather than a uniform threshold, λ_1 should be selected to be adaptive to the scale and context of the fringe image. Note that not all scales have both the fringe and object texture components. For those scales with only object texture component (such as scale 5 in Fig. 2), the traditional uniform threshold can still be used. So for these scales,

$$\hat{y}_1 = H_{\lambda_1}(r_1) = \{r_1\ if\ |r_1| > \lambda_1\ and\ 0\ otherwise\}, \tag{14}$$

where $\lambda_1 = \sqrt{2logM}\zeta$ is the universal threshold; M is the total number of data; and ζ is the standard deviation of the noise N. For the scales that contain both fringe and object texture components (such as scale 3 and 4 in Fig. 2), it is noted that,

$$r_1 = y_1 + \Phi_1 \tilde{Y}_2 + \Phi_1 Y_n = y_1 + \tilde{y}_2 + n_1, \tag{15}$$

where $\tilde{y}_2$ and n_1 are the TQWT coefficients of $\tilde{Y}_2$ and noise, respectively. So our target is to find a way to remove $\tilde{y}_2 + n_1$ from r_1 as much as possible to get a good estimation of y_1. Note that while y_2 represents the TQWT coefficients of the fringe pattern, the estimation error of y_2, i.e. $\tilde{y}_2$, also has a fringe-like structure. So if we stack each term in (15) into a matrix form, $\tilde{y}_2$ will have a much lower rank than that of r_1 because of its repetitive characteristics. That is,

$$\rho = rank(\tilde{y}_2) \ll rank(r_1). \tag{16}$$

Then $\tilde{y}_2$ can be estimated by solving the following optimization problem,

$$\tilde{y}_2^{\rho} = \underset{\tilde{y}_2}{\arg\min}\|r_1 - \tilde{y}_2\|_F \quad s.t.\ \ rank(\tilde{y}_2) \le \rho, \tag{17}$$

where $\|x\|_F$ is the Frobenius norm of x. By using the singular-value decomposition (SVD), r_1 can be factorized as $r_1 = U\Sigma V^T$, where $\Sigma = \mathrm{diag}(\sigma_1, \dots, \sigma_n)$ are the singular values of r_1 such that $\sigma_1 \ge \cdots \ge \sigma_n$. Based on the Eckart–Young–Mirsky

theorem [40], (17) can be solved analytically by,

$$\tilde{y}_2^{\rho} = U\eta_{\rho}(\Sigma)V^T, \tag{18}$$

where $\eta_{\rho}(\Sigma) = diag(\sigma_1, \dots, \sigma_{\rho}, 0, \dots, 0)$. The operator $\eta_{\rho}(\Sigma)$ sets the diagonal elements in Σ to zero except the first ρ singular values. Then a rough estimation of y_1 can be obtained as follows:

$$\tilde{y}_1^{\rho} = r_1 - \tilde{y}_2^{\rho}. \tag{19}$$

As mentioned above, $\tilde{y}_1^{\rho}$ is just a rough estimate of y_1. It can be noisy and include the error of the low rank estimation process. Fig. 4 gives an illustration of the above. In the figure, the plots of a column of r_1, y_1, and $\tilde{y}_1^{\rho}$ at the first and second iteration are shown. It can be seen in the upper plot that the sinusoidal fringe in $\tilde{y}_1^{\rho}$ is largely suppressed after the subtraction in (19). To further reduce the remaining fringe pattern, a uniform threshold can be applied. Since y_1 is sparse, we can make use of the robust statistics to determine the threshold value as [41],

$$\lambda_1 = MAD/0.6745, \tag{20}$$

where MAD is the median of the absolute value of $\tilde{y}_1^{\rho}$. Then the final $\hat{y}_2$ is obtained by a hard thresholding operation as follows:

$$\hat{y}_1 = H_{\lambda_1}(\tilde{y}_1^{\rho}) = \{\tilde{y}_1^{\rho}\ if\ |\tilde{y}_1^{\rho}| > \lambda_1\ and\ 0\ otherwise\}. \tag{21}$$

As shown in the upper plot of Fig. 4, the resulting $\hat{y}_1$ after thresholding contains very small amount of fringe data. $\hat{y}_1$ is then sent to the next stage to further enhance with the transform base Φ_2. After completing the first iteration, the residue fringe image r_1 becomes very close to y_1 as shown in the lower plot of Fig. 4. It can be seen that the blue line almost coincides with the red line. The uniform threshold determined by (20) becomes a very small value so as not to too much affect the already rather accurate $\hat{y}_1$. For this particular case, in fact only one iteration is sufficient to obtain the desired solution. By means of (14), (19) and (21), a thresholding scheme which is adaptive to the scale and context of the fringe image is designed.

The way to determine the rank ρ in (16) deserves further

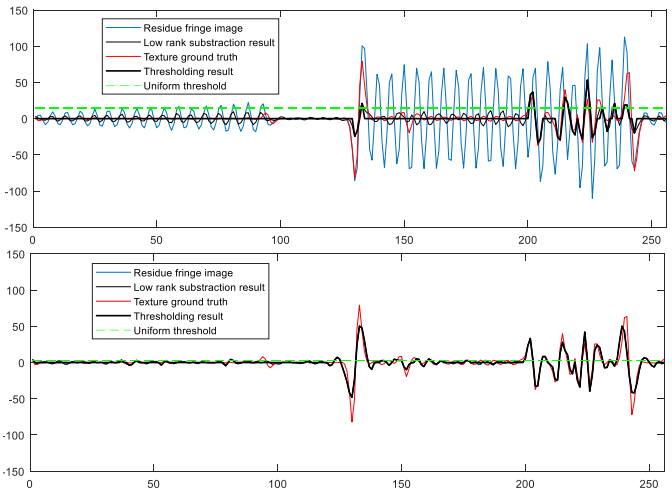

Fig. 4. A plot of a column of the wavelet transform of the residue fringe image r_1(blue line), the texture ground truth y_1 (red line), the low rank subtraction result $\tilde{y}_1^{\rho}$ (thin black line), the uniform threshold λ_i (green dash line), and the resulting texture $\hat{y}_1$ (thick black line) in the first (top) and second (bottom) iteration. The object is the one in Fig. 2.

elaboration. Note that the target here is to find a ρ such that the estimated $\tilde{y}_2^{\rho}$ will give the best $\hat{y}_1$ in (11). Although we do not know the true y_1, some properties of it can be found by looking at its probability density function (pdf) across scales. They will guide us to find the best ρ. Since y_1 is just the TQWT transform of a normal texture image, a good approximation of its marginal density can be achieved by a generalized Gaussian distribution [42-44]. For y_1 at a particular scale, its pdf can be defined as,

$$p(y_1; \alpha, \beta) = \frac{\beta}{2\alpha\Gamma(1/\beta)} \exp\left(-\frac{|y_1|}{\alpha}\right)^{\beta}, \tag{22}$$

where $\Gamma(\cdot)$ is the Gamma function. In (22), α and β model the shape of the pdf of y_1 at that scale. So the optimal ρ should be the one that can give a $\hat{y}_1$ such that its α and β are closest to those of y_1. Mathematically, it can be written as follows:

$$\rho_{opt} = \arg\min_{\rho} |\beta_{\rho} - \beta| + |\alpha_{\rho} - \alpha|, \tag{23}$$

where α_{ρ} and β_{ρ} are the α and β of the resulting $\hat{y}_1$ when a particular ρ is chosen. To solve (23), we need to know α and β. They can be estimated based on the pdf of the observed fringe image in the TQWT domain. As shown in the third row of Fig. 2, the shapes of the histograms at different scales of the object texture y_1 actually are similar (as can be seen from the values of α and β at different scales). However, it is not the case if there exists fringe patterns on y_1 (see the first row of Fig. 2). So α and β can be estimated from the histogram of the TQWT of the fringe image at the scales that do not have fringe pattern (such as scale 5 in Fig. 2). Then the parameter ρ_{opt} can be obtained by solving (23) with a binary-search algorithm over the sorted elements of matrix Σ. It is fast, with the worst logarithmic time complexity $O(\log \rho)$.

After discussing the method to obtain λ_1, let us consider the threshold λ_2. Similar to r_1, r_2 can also be defined as,

$$r_2 = y_2 + \tilde{y}_1 + n_2, \tag{24}$$

where $\tilde{y}_1$ and n_2 are the DCT coefficients of $\tilde{Y}_1$ and noise, respectively. Unlike TQWT, the DCT coefficients of the fringes, i.e. y_2, usually concentrate around a certain frequency band due to their narrow band nature. They are much sparse and have larger magnitudes than $\tilde{y}_1$. So the uniform threshold used in the traditional MCA can be applied. λ_2 should be set proportional to $\tilde{y}_1 + n_2$, which can be determined through the total estimation error R_T defined as follows:

$$R_T = \tilde{Y}_1 + \tilde{Y}_2 + N = Y - \Phi_1^T\hat{y}_1 - \Phi_2^T\hat{y}_2. \tag{25}$$

As defined in (25), R_T is the total error in the previous estimations of Y_1 and Y_2 plus noise. Since Y, $\hat{y}_1$ and $\hat{y}_2$ are known, R_T can be easily obtained by (25). Then based on R_T, we can estimate $\tilde{y}_1 + n_2$ as follows:

$$\tilde{y}_1 + n_2 = \Phi_2(R_T - \tilde{Y}_2) \cong \Phi_2(R_T - \Phi_1^T\tilde{y}_2^{\rho}). \tag{26}$$

$\tilde{y}_2^{\rho}$ in (26) is obtained in (18). Hence the threshold λ_2 can be set as,

$$\lambda_2 = \left\|\Phi_2(R_T - \Phi_1^T\tilde{y}_2^{\rho})\right\|_{\infty}. \tag{27}$$

where $\|x\|_\infty$ is the infinite norm of x, i.e. the maximum of $|x|$. Then the final $\hat{y}_2$ is obtained by a hard thresholding operation as follows:

$$\hat{y}_2 = H_{\lambda_2}(r_2) = \{r_2 \; if \; |r_2| > \lambda_2 \; and \; 0 \; otherwise\}. \quad (28)$$

Note that λ_2 is uniform to all r_2. Here we have made a mild assumption that the noise component n_2 is not so strong that $\|\tilde{y}_1 + n_2\|_\infty$ is smaller than $\|y_2\|_\infty$. To further increase the rate of convergence, the DCT coefficients at frequencies lower than a constant are ignored when determining the threshold λ_2 and also in the final $\hat{y}_2$. It is because the fringes are basically narrow band signals which do not have too low frequency components. Such constant can be determined during the initial calibration after the frequency of the fringe is determined.

The proposed **MCA algorithm for FPP** is summarized in **Algorithm I**. Fig. 5 shows the estimation results of the proposed algorithm at the first, second, fourth and the final iteration. It can be seen that on the estimated object texture (top row) the fringe pattern gradually diminishes. At the same time, the magnitude of the object's texture also gradually reduces as shown on the estimated fringe pattern (lower row).

Algorithm I. MCA algorithm for FPP

Inputs: A channel of the captured fringe image $Y \equiv G_n$ in (5);

Output: A channel of the texture image $Y_1 \equiv A_n$ and a channel of the fringe image $Y_2 \equiv G_n'$ in (5)

1: **Initialize** $\hat{Y}_1^{(0)} = 0, \hat{Y}_2^{(0)} = 0, k = 1$

2: **Repeat** until converged

3: Compute $R_1^{(k)} = Y - \hat{Y}_2^{(k-1)}$ and generate its TQWT coefficient $r_1^{(k)} = \Phi_1 R_1^{(k)}$

4: For scales contain both the fringe and object texture components, compute $\tilde{y}_1^\rho$ based on (19) and then determine λ_1 as in (20).

5: Obtain $\hat{Y}_1^{(k)} = \Phi_1^T \left(H_{\lambda_1}\left(\tilde{y}_1^\rho\right)\right)$, where $H_{\lambda_1}(.)$ is the hard thresholding operator defined in (21).

6: Compute $R_2^{(k)} = Y - \hat{Y}_1^{(k)}$ and generate its DCT coefficient $r_2^{(k)} = \Phi_2 R_2^{(k)}$.

7: Compute $R_T^{(k)} = Y - \hat{Y}_1^{(k)} - \hat{Y}_2^{(k-1)}$ and determine $\lambda_2 = \left\|\Phi_2\left(R_T^{(k)} - \Phi_1^T \tilde{y}_2^\rho\right)\right\|_\infty$ as in (27).

8: Obtain $\hat{Y}_2^{(k)} = \Phi_2^T \left(H_{\lambda_2}\left(r_2^{(k)}\right)\right)$, where $H_{\lambda_2}(.)$ is the hard thresholding operator defined in (28).

9: $k = k + 1$.

IV. Experimental Results

For testing the performance of the proposed algorithm, we implemented an FPP system using a DLP projector and a digital SLR camera. The camera has a 22.0×14.7 mm APSC sensor and a 17-55 mm lens, and the projector has a 2000:1 contrast ratio with a light output of 3000 lumens. Both devices were connected to a computer with a 3.4 GHz CPU and 16 GB RAM. They were placed at a distance of 700 – 1000 mm from the target object. The resolution of the testing fringe images was cropped to 1024×1024 pixels to simplify the TQWT processing. For all our experiments, a single fringe pattern mixed with fringes of color red, green and blue is projected unto the object.

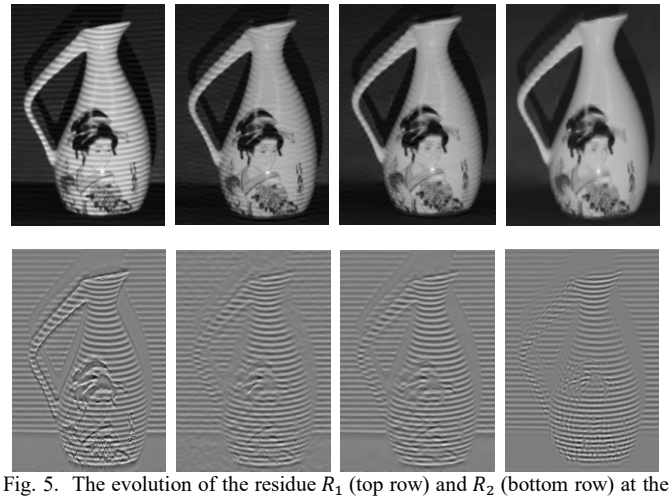

Fig. 5. The evolution of the residue R_1 (top row) and R_2 (bottom row) at the first, second, and fourth iteration and the final result Y_1 (top row, last column) and Y_2 (bottom row, last column) of a jar with strong texture (column 4 in Fig. 10). It is the result of one of the channels.

Then the captured color image is separated into 3 images (channels) by the red, green, and blue color filters of the camera. Each fringe image (channel) is then fed individually into the proposed MCA algorithm to extract the fringe pattern deformed by the object 3D profile. After the 3 fringe patterns are retrieved, the traditional PSP will be applied to reconstruct the 3D profile of the object.

A. Quantitative Evaluation

To verify the proposed method, we first conducted a quantitative evaluation by measuring the 3D profile of a flat shiny board as shown in Fig. 6 (left). The dimensions of the board are 45 cm × 35 cm. Since the board is flat, its 3D profile is exactly known. This allows us to perform objective comparisons of the accuracies of different methods. Different single-shot FPP methods were compared, including the conventional color-encoding phase-shifting profilometry (CPSP), Fourier-transform profilometry with the bias-removal strategy (FTP-BR) [1], CPSP with the conventional MCA (CPSP-MCA) [14] and the proposed method. All methods employ the simple Goldstein phase-unwrapping algorithm with a small marker placed at the center of the fringe image as the reference. While CPSP is the conventional approach, FTP-BR serves as a recently proposed single-shot approach that can address the bias in the fringe image due to the textured surface. To further understand the importance of the proposed MCA in CPSP, we compared with CPSP-MCA, which is actually a direct implementation of the conventional MCA in CPSP. In

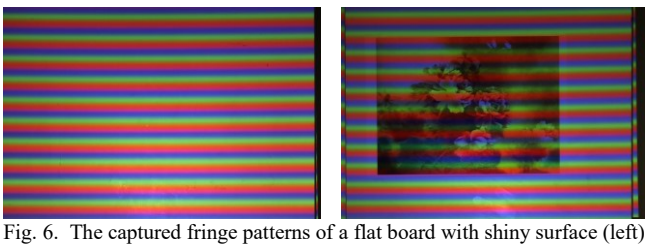

Fig. 6. The captured fringe patterns of a flat board with shiny surface (left) and flower pattern surface (right).

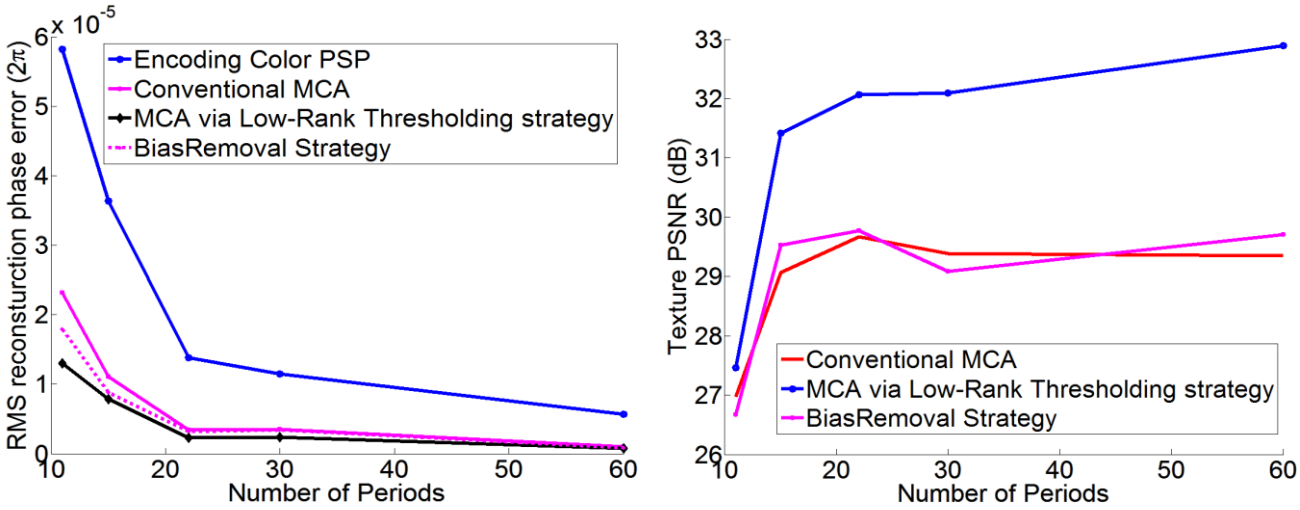

Fig. 7. Experimental results of different single-shot FPP methods on a shiny flat board

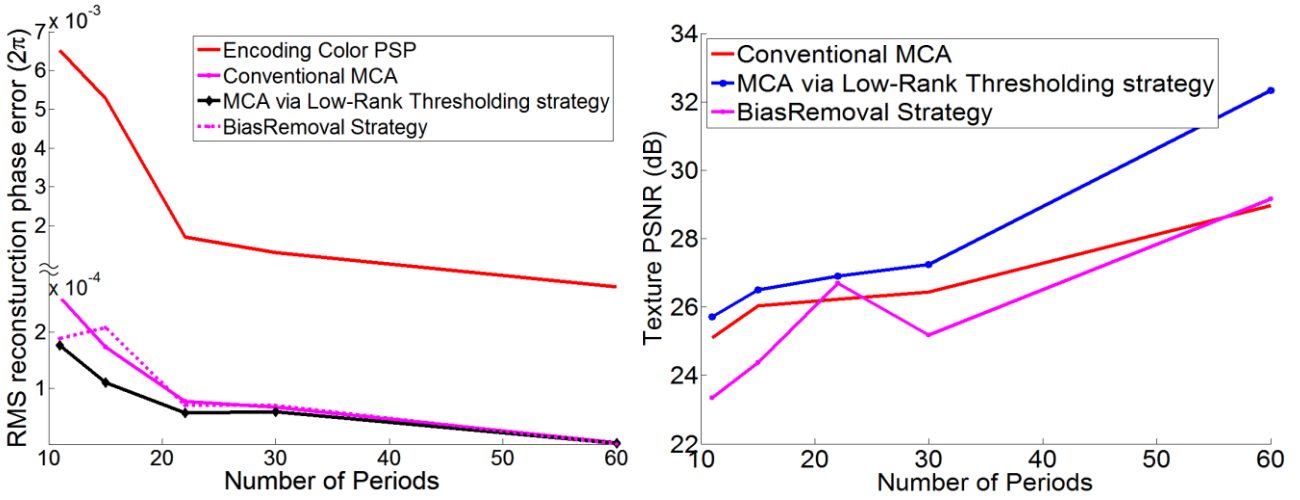

Fig. 8. Experimental results of different single-shot FPP methods on a shiny flat board with flower pattern.

this experiment, a color-encoded fringe pattern was projected onto the flat board and a camera captured the reflected image 50 times. The total number of reconstruction points is 1,008,016, ignoring a few pixels at the boundary that contain some artifacts. The error of the reconstructed phase value at each point was evaluated. The errors over the whole surface was then averaged and expressed as a root mean square (RMS) value. Fig. 7 shows the results of the compared methods when fringe patterns of different frequencies are used. As shown in the left figure, the conventional CPSP has the lowest accuracy. Apparently, any bias-removal strategy or MCA can improve the accuracy of the measured 3D profile significantly, whereas the proposed algorithm outperforms all other compared approaches consistently. In addition, unlike conventional MCA, it is also fast and requires only a few iterations.

A side benefit of the MCA method is that it can also recover the object texture during the iteration. Most of the existing single-shot FPP methods, including CPSP, do not have such feature. To allow a comparison of the proposed approach in recovering the object texture, we assume the bias-removal approach in [1] will allow the object texture to be recovered by subtracting the extracted fringe pattern from the fringe image. In this case, we have two methods to compare with and the results are shown in Fig. 7 (right) in terms of the peak signal-to-noise ratio (PSNR) of the texture image. As expected, all compared approaches cannot estimate the textured surface accurately. Once the proposed MCA is applied to CPSP, the PSNR improves significantly over all other approaches.

To further verify the robustness of the proposed method, a flower pattern paper is attached to the flat board as shown in Fig. 6 (right). It introduces further difficulty in extracting the fringe pattern from the captured fringe image. The previously mentioned experiments are then repeated with the flat board with flower pattern. Fig. 8 shows the results of the compared method when fringe patterns of different frequencies are used. As shown in the left figure, the proposed algorithm outperforms all competing approaches in reconstructing the 3D profile of the flat board. And, as shown in Fig. 8 (right), the proposed algorithm can improve the PSNR of the extracted image significantly over all other approaches. We will see in the next section that the improvement of the proposed algorithm will be even higher when the object is not just a simple flat board.

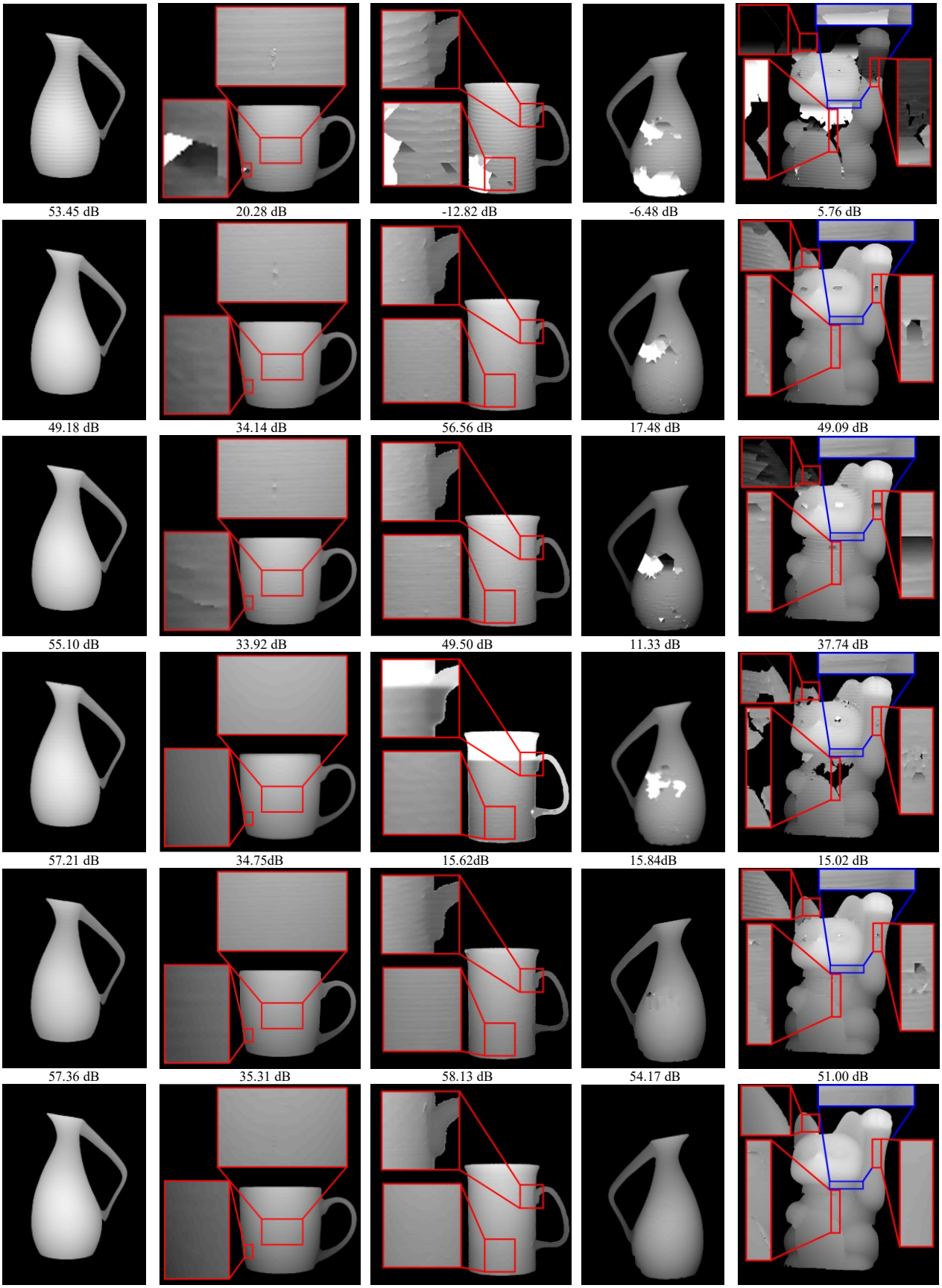

Fig. 9. 3D reconstructions of various objects with different textures. (First row) Results of CPSP; (second row) results of FTP-BR[1]; (third row) results of CPSP-MCA[14]; (fourth row) CPSP-NLO [23]; (fifth row) results of the proposed method; (sixth row) the ground truths.

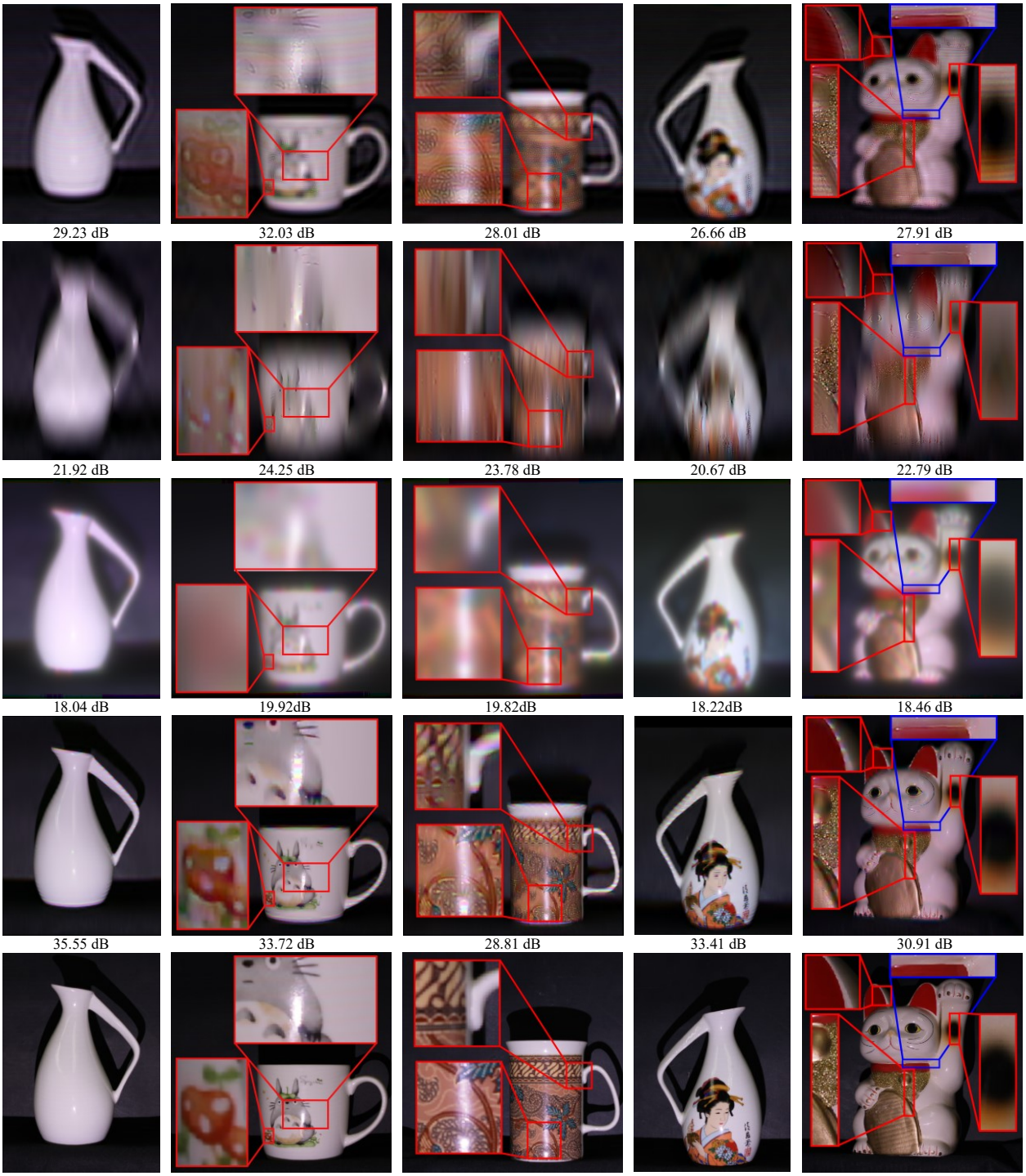

Fig. 10. Object textures obtained by different methods: (first row) results of FTP-BR[1]; (second row) results of the CPSP-MCA[14]; (third row) the CPSP-NLO [23]; (fourth row) results of the proposed method; (fifth row) the ground truths.

B. Qualitative Evaluation

We further tested the proposed algorithm in a real working environment. Six objects with various textured surfaces, shown in Fig. 10, were considered. The first object is a ceramic jar that has a mono-color surface and high reflectivity index (first column). The second object is a ceramic cup with a relatively weak textured pattern (second column). The third object has strong texture covering almost the entire object (third column). The fourth object is a jar covered with some vivid textural patterns (fourth column). Finally, a ceramic cat statue with strong texture was used (last column). It has a complex shape and large curvature region. They introduce greater difficulty to all methods when measuring their 3D profile.

Similar to the previous experiment, we compared the

proposed method with CPSP, FTP-BR, and CPSP-MCA. We also compare with a recent method, namely CPSP with non-linear optimization (CPSP-NLO) [23]. The CPSP-NLO method interpolates the peak intensities of the fringe pattern image to estimate the initial texture image. It is then used to compute the fringes pattern and depth information. Finally, a non-linear optimization is performed to smooth both the initial texture and depth image. The performances of different approaches in 3D measurement are depicted in Fig. 9. In this comparison, we generated the ground truths by scanning the scenes using 50 projections of color-encoded fringe patterns (see the last row of Fig. 9 and Fig. 10). As shown in Fig. 9(first row), the resulting 3D models generated by CPSP are erroneous for objects with textured surfaces (2nd, 3rd, 4th and 5th objects), particularly for highly textured surfaces (3rd, 4th and 5th objects). When an object contains vivid textures, the captured fringe image will have various artifacts due to color crosstalk and bias from the texture. Although the 1st object has a high SNR value, small irregular distortions can be seen due to the phase error resulting from the arbitrary object's surface reflectivity. For the 2nd object, the texture is relatively weak and hence only a few artifacts can be found. For the 3rd object, the surface is almost completely covered by strong texture. Hence, it introduces inconsistent discontinuities in the wrapped phase. For the 4th and 5th object, some dark areas and strong colors can be found on the object surface. Hence, some fringes have either nearly zero amplitude or abrupt bias that make the amplitudes of the colored sinusoids change differently. They all contribute to the errors when using the CPSP method. As shown in Fig. 9 (fourth row), the resulting 3D models generated by CPSP-NLO is superior for object with solid texture (1st object) and weak texture (2nd object) but will give erroneous results for objects with highly textured surfaces (3rd, 4th and 5th objects). The initial texture interpolation often fails since finding the peak intensities of fringes is affected by the presence of vivid texture.

Unlike CPSP and CPSP-NLO, the other comparing methods (FTP-BR, CPSP-MCA, and the proposed method) have been implemented with sparse regularization. It enhances the imperfect fringe images such that the true phase can be better recovered, as shown in Fig. 9 (2nd, 3rd, 4th and 5th objects). However, both FTP-BR and CPSP-MCA gives erroneous results when the objects contain vivid textured areas, as depicted in Fig. 9 (4th and 5th objects). And in fact, some small distortions can still be perceptible in the 2nd, 3rd, 4th and 5th objects as shown in Fig. 9. On contrary, the proposed MCA method removes most of the errors in the reconstructed 3D model; the SNRs measured against the ground truths are also the highest comparing with all other approaches. While FTP-BR has many free parameters to determine empirically and CPSP-MCA can have a long iteration time, the proposed MCA method is obviously a better choice for single-shot FPP problems. A summary of the execution time required by different approaches is given in Table I.

For the recovered object textures, FTP-BR, CPSP-MCA, and CPSP-NLO can only give blurry images as can be seen in the 1st, 2nd, 3rd row of Fig. 10. The result given by FTP-BR is blurry because there is no simultaneous texture estimation during each iteration. The textured surface is obtained by just subtracting the extracted fringe pattern from the fringe image at the end of the process. So there is no control over the accuracy of the recovered object texture. Similarly, the non-linear optimization method used to smooth the initial texture estimation in CPSP-NLO will also introduce blurred texture. It should be noticed that even in CPSP-MCA, the resulting object texture is also blurry. It is due to the inaccurate uniform threshold used during the iteration. The same problem does not exist in the proposed MCA method since, using the low-rank approximation, the optimum threshold can be estimated to achieve a good separation of the fringe and texture images. The performance can be clearly seen in Fig. 10 (fourth row). They are very close to the ground truths.

TABLE I
COMPARISON OF EXECUTION PERFORMANCE

Methods	Approximation Time Cost (s)	Remarks
FTP-BR[1]	71.77	The maximum iteration is set to be 5
CPSP-NLO [23]	398.50	The optimization is performed by utilizing the Levenberg-Marquardt method in Matlab with maximum 7 iterations as in [23]
CPSP-MCA[14]	138.32	The maximum iteration is set to be 50 with linearly decreasing threshold toward zero.
Proposed Method	38.71	It requires approximately 3-10 iteration to converge

V. CONCLUSION

In this research, we proposed a new single-shot fringe projection profilometry (FPP) algorithm that can separate the fringe pattern and object texture of a fringe image to allow robust three-dimensional (3D) measurements. The new algorithm employs a conventional color-encoding PSP such that only a single RGB fringe image needs to be projected. The key ingredient of the proposed algorithm is an improved morphological component analysis (MCA) method designed particularly for FPP problems. For the proposed MCA method, a low-rank approximation is performed to tune the optimum threshold during the iterations. This thresholding scheme differs from the traditional ones in the sense that it is adaptive and contextual. It does not require many additional hand-tuning parameters. In addition, it does not need a very good initial guess as in other approaches to guarantee the convergence. Experimental results have demonstrated the effectiveness of the proposed algorithm for simultaneously measuring the 3D profile and texture of an object. We believe that the proposed method will open many new applications for single-shot FPP where simultaneous depth and image sensing are needed.

ACKNOWLEDGEMENT

The authors would like to thank Prof. Ivan Selesnick for making the TQWT codes available online, the associate editor, and three anonymous reviewers for providing us with valuable comments and insightful suggestions which have improved this manuscript.

REFERENCES

[1] W. W.-L. Ng and D. P.-K. Lun, "Effective bias removal for fringe projection profilometry using the dual-tree complex wavelet transform," *Appl. Opt.,* vol. 51, no. 24, pp. 5909-5916, 2012.

[2] Z. Song, R. Chung, and X.-T. Zhang, "An Accurate and Robust Strip-Edge-Based Structured Light Means for Shiny Surface Micromeasurement in 3-D," *IEEE Trans. Ind. Electron.,* vol. 60, no. 3, pp. 1023-1032, 2013.

[3] G. Sansoni, S. Corini, S. Lazzari, R. Rodella, and F. Docchio, "Three-dimensional imaging based on Gray-code light projection: characterization of the measuring algorithm and development of a measuring system for industrial applications," *Appl. Opt.,* vol. 36, no. 19, pp. 4463-4472, 1997/07/01 1997.

[4] J. A. G. Albertazzi, A. C. Hofmann, A. V. Fantin, and J. M. C. Santos, "Photogrammetric endoscope for measurement of inner cylindrical surfaces using fringe projection," *Appl. Opt.,* vol. 47, no. 21, pp. 3868-3876, 2008/07/20 2008.

[5] T.-W. Hui and G. K.-H. Pang, "3-D Measurement of Solder Paste Using Two-Step Phase Shift Profilometry," *IEEE Trans. Electron. Packag. Manuf.,* vol. 31, no. 4, pp. 306-315, 2008.

[6] R. R. Garcia and A. Zakhor, "Consistent Stereo-Assisted Absolute Phase Unwrapping Methods for Structured Light Systems," *IEEE J. Sel. Topics Signal Process.,* vol. 6, no. 5, pp. 411-424, 2012.

[7] F. Sadlo, T. Weyrich, R. Peikert, and M. Gross, "A practical structured light acquisition system for point-based geometry and texture," presented at the Eurographics/IEEE VGTC Symp. Proc. Point-Based Graphics, 2005.

[8] Y. Zhang, Z. Xiong, Z. Yang, and F. Wu, "Real-Time Scalable Depth Sensing With Hybrid Structured Light Illumination," *IEEE Trans. Image Process.,* vol. 23, no. 1, pp. 97-109, 2014.

[9] Y. Wang, K. Liu, Q. Hao, D. L. Lau, and L. G. Hassebrook, "Period Coded Phase Shifting Strategy for Real-time 3-D Structured Light Illumination," *IEEE Trans. Image Process.,* vol. 20, no. 11, pp. 3001-3013, 2011.

[10] P. Cong, Z. Xiong, Y. Zhang, S. Zhao, and F. Wu, "Accurate Dynamic 3D Sensing With Fourier-Assisted Phase Shifting," *IEEE J. Sel. Topics Signal Process.,* vol. 9, no. 3, pp. 396-408, 2015.

[11] Y. Wang, K. Liu, Q. Hao, X. Wang, D. L. Lau, and L. G. Hassebrook, "Robust Active Stereo Vision Using Kullback-Leibler Divergence," *IEEE Trans. Pattern Anal. Mach. Intell.,* vol. 34, no. 3, pp. 548-563, 2012.

[12] S. Zhang and S.-T. Yau, "High-resolution, real-time 3D absolute coordinate measurement based on a phase-shifting method," *Opt. Express,* vol. 14, no. 7, pp. 2644-2649, 2006.

[13] T. Petković, T. Pribanić, and M. Đonlić, "Single-Shot Dense 3D Reconstruction Using Self-Equalizing De Bruijn Sequence," *IEEE Trans. Image Process.,* vol. 25, no. 11, pp. 5131-5144, 2016.

[14] M. Elad, J.-L. Starck, P. Querre, and D. L. Donoho, "Simultaneous cartoon and texture image inpainting using morphological component analysis (MCA)," *Applied and Computational Harmonic Analysis,* vol. 19, no. 3, pp. 340-358, 2005.

[15] Budianto and D. P. K. Lun, "Robust Fringe Projection Profilometry via Sparse Representation," *IEEE Trans. Image Process.,* vol. 25, no. 4, pp. 1726-1739, 2016.

[16] W. Lohry and S. Zhang, "High-speed absolute three-dimensional shape measurement using three binary dithered patterns," *Opt. Express,* vol. 22, no. 22, pp. 26752-26762, 2014/11/03 2014.

[17] M. Takeda and K. Mutoh, "Fourier transform profilometry for the automatic measurement of 3-D object shapes," *Appl. Opt.,* vol. 22, no. 24, pp. 3977-3982, 1983.

[18] T.-C. Hsung, D. Pak-Kong Lun, and W. W. L. Ng, "Efficient fringe image enhancement based on dual-tree complex wavelet transform," *Appl. Opt.,* vol. 50, no. 21, pp. 3973-3986, 2011.

[19] B. Budianto, P. K. D. Lun, and T.-C. Hsung, "Marker encoded fringe projection profilometry for efficient 3D model acquisition," *Appl. Opt.,* vol. 53, no. 31, pp. 7442-7453, 2014.

[20] W.-H. Su, "Color-encoded fringe projection for 3D shape measurements," *Opt. Express,* vol. 15, no. 20, pp. 13167-13181, 2007/10/01 2007.

[21] B. Budianto and D. P. K. Lun, "Inpainting For Fringe Projection Profilometry Based on Geometrically Guided Iterative Regularization," *IEEE Trans. Image Process.,* vol. 24, no. 12, pp. 5531-5542, 2015.

[22] B. Shi, B. Zhang, F. Liu, J. Luo, and J. Bai, "360° Fourier Transform Profilometry in Surface Reconstruction for Fluorescence Molecular Tomography," *IEEE J. Biomed. Health Inform.,* vol. 17, no. 3, pp. 681-689, 2013.

[23] H. Hyowon, P. Jaesik, and K. In So, "Dense Depth and Albedo from a Single-Shot Structured Light," in *Proc. Int. Conf. 3D Vision (3DV)*, 2015, pp. 127-134.

[24] H. Guo, "3-D Shape Measurement Based on Fourier Transform and Phase Shifting Method," Doctor of Philosophy, Mechanical Eng., Stony Brook University, NY, 2009.

[25] H. Guo and P. S. Huang, "3-D shape measurement by use of a modified Fourier transform method," in *Proc. SPIE 7066, Two- and Three-Dimensional Methods for Inspection and Metrology VI*, 2008, vol. 7066, pp. 70660E-70660E-8.

[26] Q. Kemao, H. Wang, and W. Gao, "Windowed Fourier transform for fringe pattern analysis: theoretical analyses," *Appl. Opt.,* vol. 47, no. 29, pp. 5408-5419, 2008.

[27] W. Gao, N. T. T. Huyen, H. S. Loi, and Q. Kemao, "Real-time 2D parallel windowed Fourier transform for fringe pattern analysis using Graphics Processing Unit," *Opt. Express,* vol. 17, no. 25, pp. 23147-23152, 2009.

[28] Z. Zhang and J. Zhong, "Applicability analysis of wavelet-transform profilometry," *Opt. Express,* vol. 21, no. 16, pp. 18777-18796, 2013/08/12 2013.

[29] J. L. Flores, J. A. Ferrari, G. García Torales, R. Legarda-Saenz, and A. Silva, "Color-fringe pattern profilometry using a generalized phase-shifting algorithm," *Appl. Opt.,* vol. 54, no. 30, pp. 8827-8834, 2015/10/20 2015.

[30] S. Ma, R. Zhu, C. Quan, B. Li, C. J. Tay, and L. Chen, "Blind phase error suppression for color-encoded digital fringe projection profilometry," *Opt. Commun.,* vol. 285, no. 7, pp. 1662-1668, 4/1/ 2012.

[31] M. Padilla, M. Servin, and G. Garnica, "Fourier analysis of RGB fringe-projection profilometry and robust phase-demodulation methods against crosstalk distortion," *Opt. Express,* vol. 24, no. 14, pp. 15417-15428, 2016/07/11 2016.

[32] C. Je, S. W. Lee, and R.-H. Park, "Color-Phase Analysis for Sinusoidal Structured Light in Rapid Range Imaging," in *Proc. 6th Asian Conf. on Computer Vision*, 2004, vol. abs/1509.04115, journals/corr/JeLP15a.

[33] J. Bobin, J. L. Starck, J. M. Fadili, Y. Moudden, and D. L. Donoho, "Morphological Component Analysis: An Adaptive Thresholding Strategy," *IEEE Trans. Image Process.,* vol. 16, no. 11, pp. 2675-2681, 2007.

[34] J. L. Starck, M. Elad, and D. L. Donoho, "Image decomposition via the combination of sparse representations and a variational approach," *IEEE Trans. Image Process.,* vol. 14, no. 10, pp. 1570-1582, 2005.

[35] J. Bobin, Y. Moudden, J. L. Starck, and M. Elad, "Morphological diversity and source separation," *IEEE Signal Process. Letters,* vol. 13, no. 7, pp. 409-412, 2006.

[36] J. Bobin, J. L. Starck, J. Fadili, and Y. Moudden, "Sparsity and Morphological Diversity in Blind Source Separation," *IEEE Trans. Image Process.,* vol. 16, no. 11, pp. 2662-2674, 2007.

[37] Z. Zhang, C. E. Towers, and D. P. Towers, "Time efficient color fringe projection system for 3D shape and color using optimum 3-frequency Selection," *Opt. Express,* vol. 14, no. 14, pp. 6444-6455, 2006/07/10 2006.

[38] P. S. Huang, Q. Hu, F. Jin, and F.-P. Chiang, "Color-encoded digital fringe projection technique for high-speed three-dimensional surface contouring," *Optical Engineering,* vol. 38, no. 6, pp. 1065-1071, 1999.

[39] I. W. Selesnick, "Wavelet Transform With Tunable Q-Factor," *IEEE Trans. Signal Process.,* vol. 59, no. 8, pp. 3560-3575, 2011.

[40] C. Eckart and G. Young, "The approximation of one matrix by another of lower rank," *Psychometrika,* vol. 1, no. 3, pp. 211-218, 1936.

[41] P. J. Huber, *Robust Statistics*. John Wiley and Sons, 1981.

[42] S. G. Chang, Y. Bin, and M. Vetterli, "Spatially adaptive wavelet thresholding with context modeling for image denoising," *IEEE Trans. Image Process.,* vol. 9, no. 9, pp. 1522-1531, 2000.

[43] S. G. Chang, Y. Bin, and M. Vetterli, "Adaptive wavelet thresholding for image denoising and compression," *IEEE Trans. Image Process.,* vol. 9, no. 9, pp. 1532-1546, 2000.

[44] M. N. Do and M. Vetterli, "Wavelet-based texture retrieval using generalized Gaussian density and Kullback-Leibler distance," *IEEE Trans. Image Process.,* vol. 11, no. 2, pp. 146-158, 2002.

Budianto (S'08) received his B.Eng. degree from Sepuluh Nopember Institute of Technology, Indonesia, M.Eng. in Information and Communication Technology from the University of Western Australia, Australia, Ph.D. degree from the Hong Kong Polytechnic University in 2003, 2009, and 2016 respectively. He is currently with the Department of Electronic and Information Engineering, the Hong Kong Polytechnic University as postdoctoral fellow. His research interests include depth sensing, sparse representation, and 3-D imaging.

Daniel P.K. Lun (SM'12) received his B.Sc.(Hons.) degree from the University of Essex, U.K., and Ph.D. degree from the Hong Kong Polytechnic University (formerly called Hong Kong Polytechnic) in 1988 and 1991, respectively. He is now an Associate Professor and Interim Head of the Department of Electronic and Information Engineering of the Hong Kong Polytechnic University. Dr Lun is active in research activities. He has published more than 130 international journals and conference papers. His research interest includes signal and image enhancement, sparse representation and applications, and 3D model reconstruction. He was the Chairman of the IEEE Hong Kong Chapter of Signal Processing in 1999-00. He was the General Co-Chair, Technical Co-Chair and the organizing committee member of a number of international conferences, including ICASSP 2003, ICIP 2010 and ICME 2017. Dr Lun is a member of the DSP and Visual Signal Processing and Communications Technical Committee of IEEE Circuits and Systems Society. He is an associate editor of the IEEE Signal Processing Letters. He is a Chartered Engineer, a Fellow of IET, a corporate member of HKIE and a senior member of IEEE.

Yuk-Hee Chan (M) received the B.Sc. (Hons.) degree in electronics from Chinese University of Hong Kong in 1987, and the Ph.D. degree in signal processing from The Hong Kong Polytechnic University in 1992. Between 1987 and 1989, he was an R&D Engineer with Elec & Eltek Group, Hong Kong. In 1992, he joined the Hong Kong Polytechnic University, where he is currently an Associate Professor in the Department of Electronic and Information Engineering. He has published more than 150 research papers in various international journals and conferences. His research interests include image and video compression, image restoration, halftoning, demosaicking, 3D measurement and fast computational algorithms in digital signal processing. Dr Chan was the Chairman of the IEEE Hong Kong Joint Chapter of CAS and COM in 2003–2004 and the Chair of the IEEE Hong Kong Section in 2015.